

Supplementary Information

Supplementing electrochemical measurement by colorimetric measurement to evaluate supercapacitor electrode

Yuanhui Su,^a Yu Huan,^{a} Wang Liu, Shuotong Wang,^b Xiaoying Guo,^a Tao Wei^{a*}*

^aSchool of Material Science and Engineering, University of Jinan, Jinan 250022, China

^bCollege of Energy, Soochow University, Suzhou 215006, China

*Corresponding Author: mse_huany@ujn.edu.cn (Yu Huan); mse_weit@ujn.edu.cn (Tao Wei).

Experimental Methods

Materials

The used chemicals were all purchased from Macklin and used as received unless noted otherwise. Activated carbon (AC, YP-50F), acetylene black, separators and coin-type cell parts were obtained from Guangdong Canrd New Energy Technology Co., Ltd.

MnO₂ was prepared by a chemical precipitation method. 1.5805 g of KMnO₄ and 3.02 g of MnSO₄ solution (50 wt%) were dispersed into 50 mL of DI water, respectively. During stirring, MnSO₄ solution was added into KMnO₄ solution drop by drop. After continuous stirring at 80 °C for 4 hours, the mixture was washed with DI water and ethanol, and dried at 60 °C for 12 h.

For the synthesis of V₂O₅, 0.585 g of NH₄VO₃ was dissolved into 30 mL of deionized water, and then the solution was transferred into a 50 mL Teflon-lined autoclave and heated at 180 °C for 24 h. Then, the as-received solid product was washed, dried, and annealed 500 °C for 5 h under the argon atmosphere.

Co(OH)₂ was prepared by a hydrothermal method. 0.56 g of hexamethylene tetramine, 5 mL of glycerine and 0.4758 g of CoCl₂·6H₂O were dissolved in 45 mL of deionized (DI) water, with constant stirring for 30 min. Then, the mixed solution was transferred to a 100 mL Teflon-lined autoclave and kept at 100 °C for 5h. After the reaction was complete, the precipitate was centrifuged DI water and ethanol several times and dried at 60 °C for 12 h.

Ni(OH)₂ was prepared by a chemical precipitation method. 5.257 g of oxalic acid and 100 μL of tween 20 were dissolved in 40 mL DI of water and heated up to 60 °C in a water bath under continuous stirring. Then, 40 mL of 1M NiSO₄ solution was added drop-by-drop to the prepared oxalic acid solution. During heating and stirring, NaOH solution (0.5 M) was added to adjust pH value to 7. The green precipitate was then washed with DI water and ethanol for several times and dried under vacuum to get the Ni(OH)₂. The NiO was obtained by annealing Ni(OH)₂ at 270 °C in air for 1 h.

A series of layered double metal hydroxides (LDH) was synthesized by coprecipitation method. Ni(NO₃)₂·6H₂O and Co(NO₃)₂·6H₂O with a Ni²⁺: Co²⁺: Fe³⁺ molar ratio of 1:2:1 were mixed in 40 mL of deionized water under magnetic stirring in 80 °C. Then, the pH of the solution was adjusted to 10 by adding NaOH solution (0.25 M). After stirring for 10 h, the resulting solution

was cooled to room temperature naturally. The product was collected, washed, and dried to obtain FeNiCo-LDH. By adjusting the metal nitrate, NiCo-LDH ($\text{Ni}^{2+} : \text{Co}^{2+} = 3:1$) and ZnCo-LDH ($\text{Zn}^{2+} : \text{Co}^{2+} = 1:2$) were prepared by the same way.

Characterization

The crystallinity and phase composition of MnO_2 samples were assessed through X-ray diffraction (XRD, Bruker D8 Advance, $\text{Cu K}\alpha$). The ultraviolet-visible diffusion reflectance spectroscopy (UV-Vis/DRS; Shimadzu UV 2600, Shimadzu, Tokyo, Japan) is employed to determine the band gap energy of pristine MnO_2 , charged MnO_2 , and discharged MnO_2 . The valence band photoelectron X-ray spectroscopy (VB-XPS) data of MnO_2 were obtained using an ESCALab 250 Xi electron spectrometer (Thermo Fisher Scientific, USA).

Electrode preparation and electrochemical measurement

Generally, all working electrode was prepared as follows: the active materials, acetylene black and PVDF were grinded and mixed in N-methylpyrrolidone (NMP) according to the weight ratio of 8:1:1 to make a slurry. Then, the above slurry was coated on current collector ($1 \times 1 \text{ cm}^2$), and dried on vacuum at $70 \text{ }^\circ\text{C}$ for 12 h. Nickel foam was used as current collector unless otherwise specified. To evaluate the degraded/failed behavior of combined MnO_2 , the combined electrode was prepared in the same way, in which three kinds of MnO_2 had an active area of $0.6 \times 0.6 \text{ cm}^2$, respectively. The $\text{Ni}(\text{OH})_2$ electrodes with different current collectors (Ni foam, Ni mesh, and carbon paper) and AC electrodes with different current collectors (Ni foam and carbon paper) were prepared as for contrast experiment.

A typical three-electrode system was used to test the electrochemical performance of supercapacitor. Pt foil was used as the counter electrode (CE). When MnO_2 was used as the working electrode (WE) in $1 \text{ M Na}_2\text{SO}_4$ electrolyte and V_2O_5 was used as the WE in LiNO_3 electrolyte, the reference electrode (RE) was Ag/AgCl electrode. $\text{Co}(\text{OH})_2$, $\text{Ni}(\text{OH})_2$, NiO, and LDH were used as the WE in 2 M KOH , and a saturated calomel electrode served as the RE. AC electrode was used as WE in 6 M KOH with Hg/HgO electrode as a RE. The conventional electrolytic tank was replaced by a cube-shaped quartz cuvette with excellent light transmission,

which allows the detecting light passing through the glass and irradiating on the surface of electrode plates.

The two-electrode system was used for electrochemical characterization of the asymmetric supercapacitor (ASC). All of the ASC were assembled in the one-side perforated 2032 coin-type cell. The perforated cathode shell of ASC was enclosed with optical quartz glass and sealed around with acrylate adhesive. The perforated structure allows the detecting light passing through the coin cell and irradiating on the surface of electrode plates. The MnO₂//AC ASC devices were fabricated with AC as negative electrode and MnO₂ as positive electrode, 1 M Na₂SO₄ as aqueous electrolytes and cellulose paper as separator. The NiCo-LDH//AC ASC and ZnCo-LDH//AC ASC were assembled in the same way as above, with the difference being that the NiCo-LDH and ZnCo-LDH electrodes as the positive electrode, respectively, and the electrolytes are 2M KOH aqueous. The mass loading of positive and negative electrode active materials was quantified by the charge balance theory.

Cyclic voltammetry test (CV) was conducted using an electrochemical analyzer (660E, CH Instruments, China). Galvanostatic charge-discharge (GCD) test, rate capability, and cycle stability of SCs were carried out on LANHE (CT2001A) battery testing system at 25 °C. The capacity value was evaluated from GCD curves according to the following Eq. (2):

$$Q_m = \frac{I\Delta t}{m} \quad (2)$$

Here, Q_m represents the specific capacity (C g⁻¹), I represents the current (A), m represents the weight of active materials (g) and Δt represents the discharge time (s).

Formulas for Converting Spectra to CIELAB Color Space

The color standard employed in this work is CIELAB color space. The CIELAB color space, developed by the International Commission on Illumination (CIE), is represented by three matrices: L^* (brightness), a^* (redness/greenness), and b^* (yellowness/blueness). On the a^* axis (-127 to +127), positive values indicate the presence of red, while negative values signify green. Similarly, on the b^* axis (-127 to +127), positive values denote yellow, whereas negative values represent blue. The L^* axis spans from the darkest black ($L^* = 0$) to the brightest white ($L^* = 100$).

To obtain color values represented in the LAB color space, the spectra are transformed into tristimulus values using the Eq. (S1).

$$\begin{cases} X = \int_{\lambda_1}^{\lambda_2} R(\lambda)s(\lambda)\bar{x}(\lambda)d\lambda \\ Y = \int_{\lambda_1}^{\lambda_2} R(\lambda)s(\lambda)\bar{y}(\lambda)d\lambda \\ Z = \int_{\lambda_1}^{\lambda_2} R(\lambda)s(\lambda)\bar{z}(\lambda)d\lambda \end{cases} \quad (\text{S1})$$

In this formula, λ is the wavelength of the equivalent monochromatic light. $R(\lambda)$ and $s(\lambda)$ are the reflectance spectrum of sample and the relative spectral power distribution of illuminant, respectively. $\bar{x}(\lambda)$, $\bar{y}(\lambda)$, and $\bar{z}(\lambda)$ are the CIE tristimulus values x , y , and z derived from the CIE standard observer, respectively ¹.

Then, the XYZ values are transform into $L^*a^*b^*$ values of LAB by Eqs. (S2) and (S3):

$$\begin{cases} f\left(\frac{X}{X_n}\right) = \begin{cases} \left(\frac{X}{X_n}\right)^{1/3}, & \frac{X}{X_n} > 0.008856 \\ 7.787037\frac{X}{X_n} + \frac{16}{116}\frac{X}{X_n}, & \frac{X}{X_n} \leq 0.008856 \end{cases} \\ f\left(\frac{Y}{Y_n}\right) = \begin{cases} \left(\frac{Y}{Y_n}\right)^{1/3}, & \frac{Y}{Y_n} > 0.008856 \\ 7.787037\frac{Y}{Y_n} + \frac{16}{116}\frac{Y}{Y_n}, & \frac{Y}{Y_n} \leq 0.008856 \end{cases} \\ f\left(\frac{Z}{Z_n}\right) = \begin{cases} \left(\frac{Z}{Z_n}\right)^{1/3}, & \frac{Z}{Z_n} > 0.008856 \\ 7.787037\frac{Z}{Z_n} + \frac{16}{116}\frac{Z}{Z_n}, & \frac{Z}{Z_n} \leq 0.008856 \end{cases} \end{cases} \quad (\text{S2})$$

$$\begin{cases} L^* = 116f\left(\frac{Y}{Y_n}\right) - 16 \\ a^* = 500\left[f\left(\frac{X}{X_n}\right) - f\left(\frac{Y}{Y_n}\right)\right] \\ b^* = 200\left[f\left(\frac{Y}{Y_n}\right) - f\left(\frac{Z}{Z_n}\right)\right] \end{cases} \quad (\text{S3})$$

Where X , Y and Z are the CIE XYZ tristimulus values of sample, and X_n , Y_n , and Z_n are the normalized CIE XYZ tristimulus values of the reference white point.

Formulas for calculating of energy band structure

The UV–Vis/DRS were recorded to determine the band gap energy of samples. The Tauc' plots i.e., $(\alpha\hbar\nu)^2$ versus photon energy ($\hbar\nu$) based on the power-law relation for samples were considered to estimate band gap (E_g) values. The E_g energy The band gap (E_g) energy could be determined by Eq. (S4) ^{2,3}:

$$\alpha\hbar\nu = A(\hbar\nu - E_g)^{\frac{n}{2}} \quad (\text{S4})$$

where α , h , ν , and A are absorption coefficient, Planck's constant, light frequency, and proportionality constant, respectively.

The VB-XPS was used to determine the valence band potential ($E_{\text{VB, XPS}}$) of samples. Then, the E_{VB} relative to the standard hydrogen electrode and corresponding conduction band potential (E_{CB}) can be calculated according to the following Eqs. (S5) and (S6):

$$E_{\text{VB}} = \varphi + E_{\text{VB, XPS}} - 4.44 \quad (\text{S5})$$

$$E_{\text{CB}} = E_{\text{VB}} - E_g \quad (\text{S6})$$

where φ is the work function of the instrument (4.72 eV).

Supplemental Figure

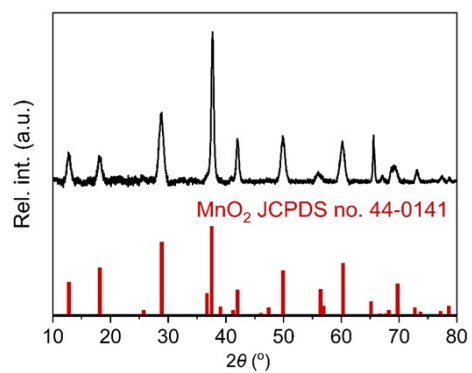


Figure S1. The XRD pattern of MnO₂. All diffraction peaks correspond to pure α-MnO₂ (JCPDS no. 44-0141), which confirms its successful synthesis.

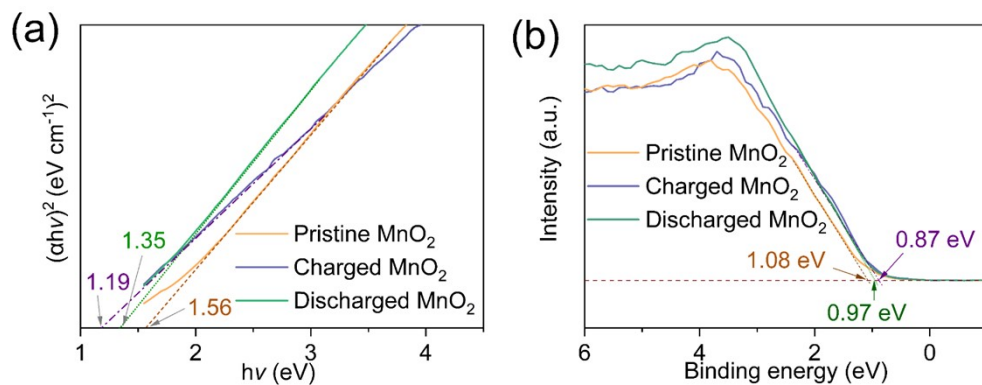


Figure S2. (a) The Tauc' plots and (b) valence band photoelectron X-ray spectroscopy (VB-XPS) spectra, of pristine MnO₂, charged MnO₂, and discharged MnO₂.

The band gap (E_g) values of MnO₂ samples were determined by the Tauc' plots and valence band photoelectron X-ray spectroscopy (VB-XPS) spectra, using Eqs. (S4 –S6). The optical E_g of pristine MnO₂, charged MnO₂, and discharged MnO₂ is taken as 1.56, 1.19, 1.35 eV, respectively. The valence band potential ($E_{\text{VB, XPS}}$) of pristine MnO₂, charged MnO₂, and discharged MnO₂ are measured to be 1.08, 0.87 and 0.97 eV, respectively. The corresponding E_{CB} is then calculated to be -0.2 , -0.04 , and -0.1 eV. According to the aforesaid results, the schematic illustration of the band structures of pristine MnO₂, charged MnO₂, and discharged MnO₂ samples is displayed.

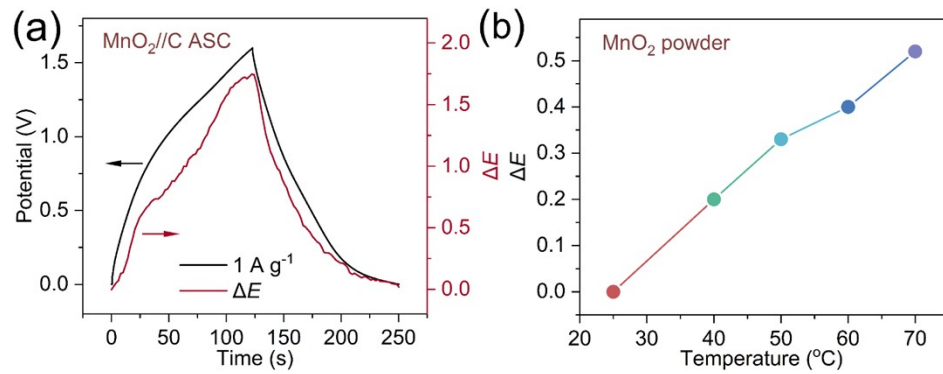


Figure S3. (a) The GCD and corresponding ΔE curves for $\text{MnO}_2//\text{AC}$ asymmetric supercapacitor at 25°C . (b) The varied ΔE values of MnO_2 powder with temperature increasing from 25 to 70°C .

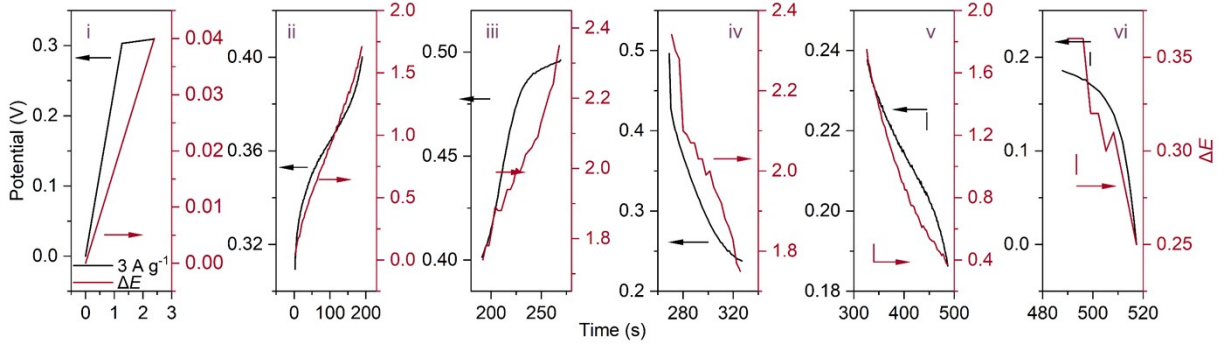


Figure S4. The GCD and corresponding ΔE curves of $\text{Ni}(\text{OH})_2$.

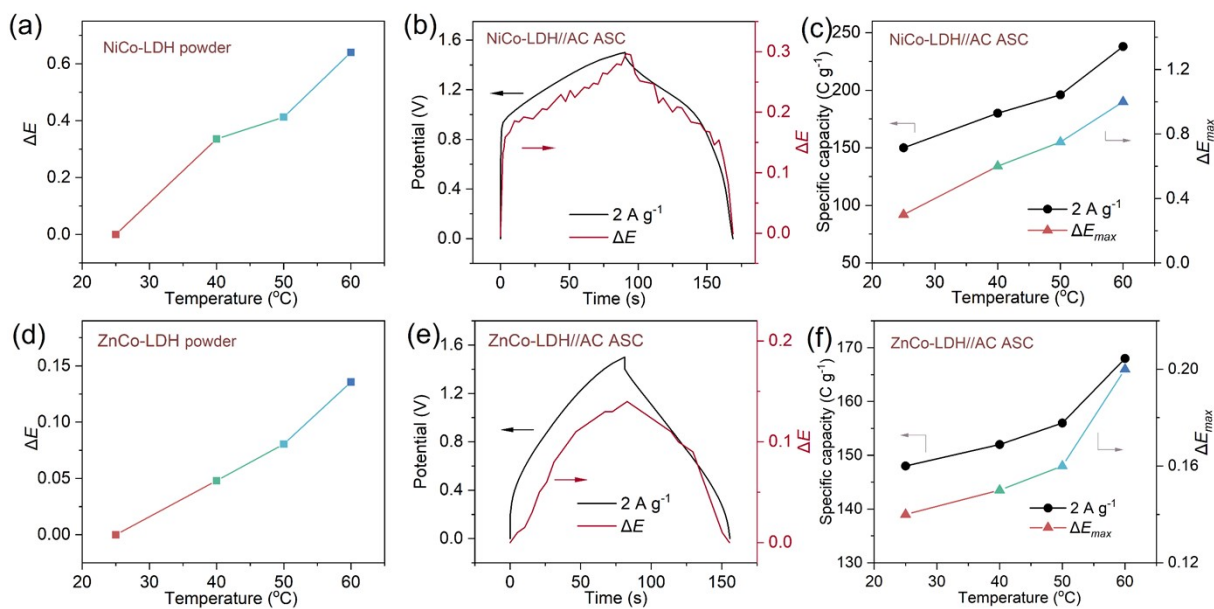


Figure S5. (a) The varied ΔE values of NiCo-LDH powder with temperature increasing from 25 to 60 °C. (b) The GCD and corresponding ΔE curves for NiCo-LDH/KOH/AC ASC at 25 °C. (c) The variations of specific capacity and corresponding ΔE_{max} curves for NiCo-LDH/KOH/AC ASC with temperature increasing from 25 to 60 °C. (d) The varied ΔE values of ZnCo-LDH powder with temperature increasing from 25 to 60 °C. (e) The GCD and corresponding ΔE curves for ZnCo-LDH/KOH/AC ASC at 25 °C. (f) The variations of specific capacity and corresponding ΔE_{max} curves for ZnCo-LDH/KOH/AC ASC with temperature increasing from 25 to 60 °C.

Here, the ΔE values of NiCo-LDH and ZnCo-LDH powder are measured within the temperature range of 25 to 60 °C. The ΔE of electrode powder increases with temperature, providing the possibility to evaluate the thermal behavior of electrode materials by colorimetric measurement. At 25 °C, the GCD curves and associated ΔE curves exhibited high reversibility. As the temperature increased, the maximum differential ΔE_{max} for both NiCo-LDH and ZnCo-LDH electrodes also increased, attributed to the enhancement of working temperature and improved energy storage capabilities at elevated temperatures.

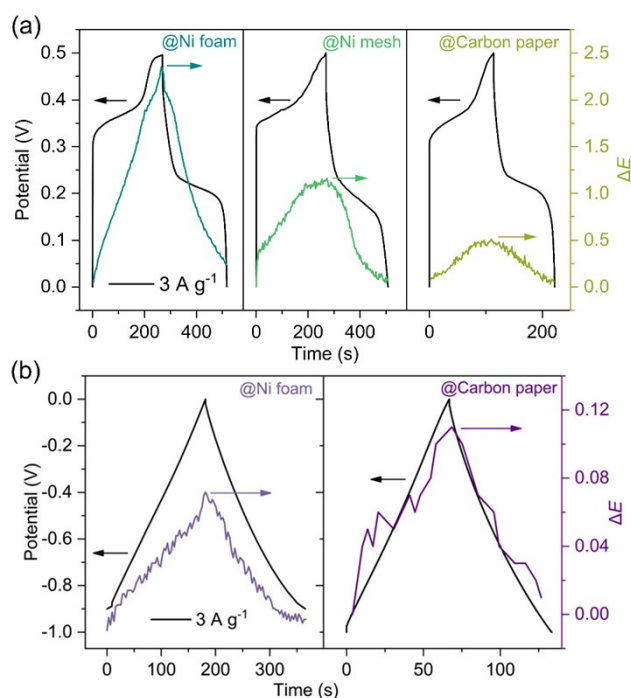


Figure S6. (a) GCD and corresponding ΔE curves of Ni(OH)₂ electrodes prepared using nickel foam, nickel mesh, and carbon paper as current collectors, tested at 3 A g⁻¹. (b) GCD and corresponding ΔE curves of AC electrodes prepared using nickel foam and carbon paper as current collectors, tested at 3 A g⁻¹.

Taking Ni(OH)₂ electrode coatings on Ni foam, Ni mesh, and carbon paper as examples, their energy storage and GCD curve show apparent variations with different current collectors. These variations also can be revealed by the varied ΔE values obtained during the charge-discharge process. The explanation for these variations lies in two primary factors: 1) reduced energy storage due to decreased accumulation of OH⁻ ions leading to reduced color differences; 2) incomplete coverage of the Ni(OH)₂ electrode materials on the surfaces of the current collectors, resulting in different colors and reflectivity that cause apparent color differences when light is reflected off them. The variability in ΔE values indicates that the impact of different current collectors on electrode energy storage can be detected using Colorimetric measurement. Further evidence supporting the generality of Colorimetric measurement comes from to distinguish the Ni foam and carbon paper while using as current collectors of AC electrode.

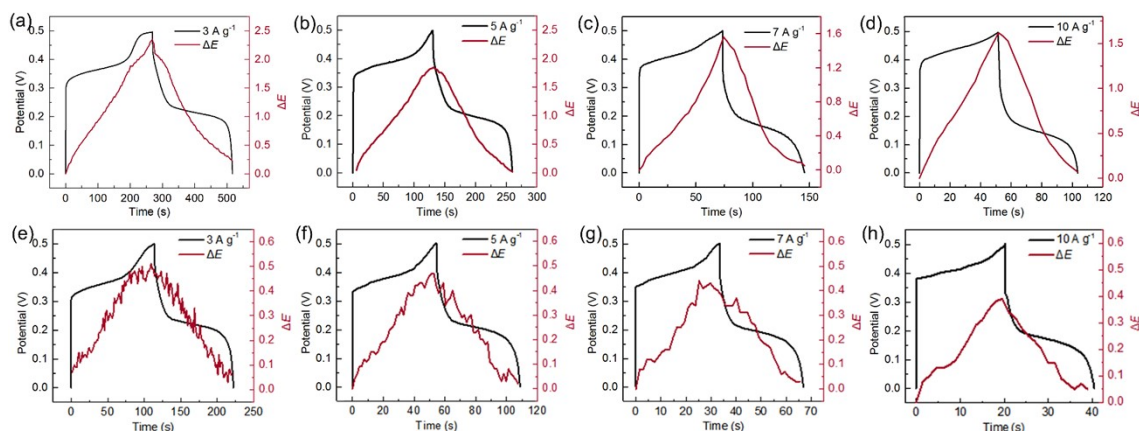


Figure S7. GCD and corresponding ΔE curves of $\text{Ni}(\text{OH})_2$ electrodes prepared using (a-d) nickel foam and (e-h) nickel mesh as current collectors, tested at current densities of (a, e) 3 A g^{-1} , (b, f) 5 A g^{-1} , (c, g) 7 A g^{-1} , and (d, h) 10 A g^{-1} .

Figure S7 shows the GCD and corresponding ΔE curves of $\text{Ni}(\text{OH})_2$ electrodes fabricated with nickel foam and nickel mesh as current collectors at various current densities (3 A g^{-1} , 5 A g^{-1} , 7 A g^{-1} , and 10 A g^{-1}). Both nickel foam and nickel mesh-based electrodes exhibit consistent ΔE decay trends with increasing current density. At 3 A g^{-1} , maximum ΔE variations are observed, indicating stable OH^- ion accumulation and uniform redox activity. However, when current density increases to $5\text{--}10 \text{ A g}^{-1}$, the ΔE values progressively decrease, mirroring the capacity fade observed in conventional electrochemical measurements. Despite structural disparities between the porous foam and mesh current collectors, the ΔE response remains proportional to specific capacity, confirming the technique's adaptability to diverse substrate architectures. The observed ΔE trends provide critical insights into electrode performance under practical conditions. These findings not only validate the colorimetric method's sensitivity to current collector properties but also highlight its potential as a non-invasive, real-time diagnostic tool for optimizing SC electrode design in industrial applications.

References

1. A. C. Harris and I. L. Weatherall, *J. Roy. Soc. New Zeal.*, 1990, **20**, 253-259.
2. J. Tauc, R. Grigorovici and A. Vancu, *phys. stat. sol.*, 1966, **15**, 627-637.
3. J. Tauc, *Mat. Resh. Bull.*, 1968, **3**, 37-46.